JOURNAL OF APPLIED ELECTROCHEMISTRY **27** (1997) 1219–1231

REVIEWS IN APPLIED ELECTROCHEMISTRY No. 47

In situ optical studies of metal deposition

I. I. SUNI
Department of Chemical Engineering, Clarkson University, Potsdam, NY 13699-5705 USA

Received 5 November 1996; revised 27 January 1997

The importance of microscopic morphological control to metal electro- and electroless deposition in several emerging technologies is discussed. The use of *in situ* optical probes of the morphological development of deposits is described. A number of these are reviewed to describe both the potential of each method and the available literature on studies of electro- and electroless deposition. Included are optical probes of the mass transfer boundary layer, X-ray diffractive and spectroscopic methods, ellipsometry, surface-enhanced Raman spectroscopy, infrared absorption spectroscopy, second harmonic generation and electroreflectance.

Keywords: *Morphological control, Electrodeposition, Electroless deposition, Optical probes, Optical methods*

1. Introduction

A number of optical techniques can be employed to investigate processes occurring on or near electrode surfaces. Authoritative reviews have been published for a variety of optical methods, including surface-enhanced Raman spectroscopy (SERS) [1–3] and infrared spectroscopy [4–6], which probe the vibrational energy levels and bonding geometries of adsorbed species, X-ray absorption and diffraction methods [7] and ellipsometry [8, 9], which probe the bond lengths and morphologies of adsorbed species, and second harmonic generation [10, 11] and photo- and electroreflectance [12–14], which probe the surface electronic properties. Optical methods such as interferometry, probe beam deflection, photothermal deflection spectroscopy and absorption spectroscopy, which probe concentration gradients in the mass transfer boundary layer, have been less thoroughly reviewed [15–17]. Such discussions have detailed the wealth of information obtained on both the chemical interactions of small molecules with metal surfaces and the electronic properties of the surface. However, no review to date has focussed on studies of metal deposition by optical methods.

Several of the optical methods listed above are capable of probing the microstructural evolution at the metal-electrolyte interface. This has traditionally been a specialized field within electrochemical engineering which is becoming increasingly important due to currently emerging applications requiring greater control of morphology. Examples include electro- and electroless deposition of noble metals for interconnects in the microelectronics industry, electrodeposition of compositionally modulated alloys (CMAs), and electro- and electroless deposition of exotic materials for microelectronics applications.

Electro- and electroless deposition of noble metals in the microelectronics industry often puts strong demands on the deposit morphology. For example, the resistivity of sub-0.25 μm noble metal interconnects will depend strongly on grain size [18] and other morphological parameters. The control of the deposit morphology cannot easily be optimized without an understanding of the physical and chemical phenomena involved. One such process which is poorly understood is surface transport. Surface diffusion on terraces during electro- and electroless deposition of noble metals probably affects both the deposition rate and the deposit morphology. Gold electrodeposition has been used in the electronics industry for a variety of applications [19–22], with soft Au usually being electrodeposited at current densities ranging from 1–8 mA cm^{-2} from a bath containing approximately 0.06 M $KAu(CN)_2$, phosphate, citrate and other additives [19, 20]. This current density is 1–3 orders of magnitude lower than that employed in most industrial plating baths, which are operated in a regime where charge transfer is rate-limiting. At such a low current density, noble metal electrodeposition is probably rate-limited by surface diffusion, as has been demonstrated by galvanostatic transients observed during Ag and Cu electrodeposition [23–28]. Electro- and electroless deposition of Cu have important potential applications for interconnect fabrication in the next generation of sub-0.25 micron microelectronics devices [29]. Electroless deposition rates are typically 1–4 μm h^{-1}, equivalent to current densities of 0.8–3.1 mA cm^{-2}. The rate-limiting step in electroless Cu deposition is the subject of some controversy [30, 31], but the low plating rate suggests that even if surface diffusion is not rate-limiting, atomic processes such as surface diffusion and nucleation will have a strong effect on deposit morphology [32]. Numerous investigators have studied the process-structure-function relationships between deposition parameters and deposit morphology [33–36].

Another developing field where morphological control can be important is electrodeposition of

compositionally modulated alloys (CMAs), which are heterostructures composed of alternating thin films of two different alloys. Such heterostructures have many potential applications, including wear resistance and electronic switching, and are currently commercially fabricated predominantly by vacuum methods such as evaporation and sputtering. Extensive research has focussed on the giant magnetoresistive effect, the large resistivity change with an applied magnetic field, exhibited by CMAs composed of alternating magnetic and nonmagnetic layers. Current research on the production of CMAs by electrodeposition [37–39] offers the potential of greatly improved economics. Such efforts are presently limited primarily by current nonuniformity, although grain boundaries and interfacial sharpness have been shown to affect electrical properties [40]. As layer thicknesses shrink below 1 nm [38], control of microscopic processes will become increasingly important. Nonintrusive optical methods for monitoring morphology development and possibly surface electronic and magnetic properties could play a vital role in pilot plant studies of this technology.

Metal electro- and electroless deposition are processes fundamental to electrochemical engineering. Although some optical methods probe electrodeposition processes directly, many of the methods discussed below were developed to investigate small molecules at the electrochemical interface. However, even these methods can often be employed to probe electrodeposition processes by a variety of ingenious indirect approaches. This paper will address the contributions of optical methods to the understanding of metal electro- and electroless deposition, focussing mainly on the information that can be obtained. Each method will be described only in enough experimental detail to describe its capabilities and limitations. A few methods have been omitted which appear to offer little promise of significant insight into metal deposition processes. Optical probes often yield complementary information to that provided by nonoptical probes such as scanning tunneling microscopy (STM) and atomic force microscopy (AFM). Although STM and AFM can more readily provide atomic-scale information on electrodeposition, they are applicable only to relatively flat surfaces, they are less compatible with realistic pilot studies, and they often cannot give interpretable information on superatomic length scales. In addition, optical probes are generally less obtrusive, as evidenced by AFM and STM studies showing that these techniques can enhance or retard electrodeposition rates [41].

2. Optical probes of the mass transfer boundary layer

A number of closely related optical techniques, including interferometry, probe beam deflection, photothermal deflection spectroscopy and absorption spectroscopy, have been developed to measure concentration gradients and investigate mass transfer in the boundary layer during metal deposition. The first three of these techniques is based on the refractive index gradients which arise near an electrode during electro- and electroless deposition from relatively dilute baths. The last, absorption spectroscopy, has the advantage of specific detection of one particular species in the boundary layer. All of these probes are capable of measuring diffusivities by monitoring the temporal evolution of the boundary layer, and several have also been employed in elegant studies of natural convection during electro- and electroless deposition. In addition, these methods are, in principle, capable of studying mass transfer in the presence of forced convection [42, 43].

Interferometry was the first technique to be widely applied to studies of concentration gradients in the mass transfer boundary layer. During electro- and electroless deposition, concentration gradients in the boundary layer produce gradients in the refractive index, which in turn cause local phase shifts. If an optical source is divided into a probe and a reference beam so that the probe beam passes through the boundary layer and the reference beam through the bulk solution, then recombination of the two beams creates an interference pattern which can be uniquely inverted to obtain the refractive index field [17]. In cases where there is a gradient of only a single component, the refractive index field can be uniquely inverted to obtain the concentration field. Interferometry becomes difficult at high current densities where the spatially dependent deflection of the probe beam complicates the interference phenomenon [44].

This phenomenon can be exploited by the method of probe beam deflection, where the deflection of a well-collimated laser which is propagating parallel to an electrode surface is measured [16]. For an n-component solution, the deflection θ is simply

$$\theta = \frac{L}{n}\sum_{i=1}^{m}\frac{\partial n}{\partial C_i}\frac{\partial C_i}{\partial x} \qquad (1)$$

where L is the path length, x is the direction perpendicular to the electrode, n is the refractive index, and C_i the species concentration. Since the resolution of commonly employed United Detector Technologies position sensitive detectors is approximately 2.5 μm, the gradient resolution limit is about 2.1×10^{-4} M cm^{-1}, assuming a typical refractive index gradient of 10^{-2} M^{-1}. This corresponds to a detection limit of approximately 7×10^{-6} M for a boundary layer 350 μm thick. A related technique, photothermal deflection spectroscopy, employs a modulated pump laser to create an a.c. temperature gradient along with the d.c. concentration gradient [15]. Thus the total beam deflection is a generalization of Equation 1,

$$\theta = \frac{L}{n}\left(\frac{\mathrm{d}T}{\mathrm{d}x}\frac{\partial n}{\partial T} + \sum_{i=1}^{m}\frac{\mathrm{d}C_i}{\mathrm{d}x}\frac{\partial n}{\partial C_i}\right) \qquad (2)$$

where the first team is created by the modulated pump laser and the second term by the electrochemical reaction. Thus, the d.c. beam deflection takes the same form as for probe beam deflection. Interfero-

metry, probe beam deflection and photothermal deflection spectroscopy all become problematic in the presence of multiple concentration gradients, which may commonly arise due, for example, to anionic migration or to cathodic accumulation of the complexing agent during deposition from highly complexing electrolytes.

If multiple concentration gradients exist in the boundary layer, then spectroscopic probes must be employed. The simplest of these direct light onto the electrode surface at an oblique angle and sample the boundary layer only over a short propagation distance. Such studies can be done in an external or internal reflectance geometry [45] or in a transmission geometry using optically transparent electrodes (OTE) [46]. In part due to the short interaction length, these methods have been used primarily to study the optical or electronic properties of the interface rather than transport phenomena. Study of the boundary layer requires optical propagation at grazing incidence [47, 48] or parallel to the electrode surface [49]. Such methods measure optical absorption either during a potential scan (voltabsorptometry) or after application of a potential step (chronoabsorptometry). The sensitivity is usually limited by mechanical stability or by fluctuations in the optical source intensity or temperature. The most sophisticated optical probe of the boundary layer involves propagation of a well-collimated laser parallel to an electrode surface in order to perform spatially resolved absorption spectroscopy. The sensitivity of this method is in many cases limited by scattered light from the monochromator or by source instability. However, in some cases source instability and thermal drift can be calibrated and monochromatic sources employed, in which case the minimum detectable absorbance may be determined by the number of photons (N_{sat}) contained in the detector well as [50]

$$A_{min} = -\log\left[1 - \left(\frac{8}{N_{sat}}\right)^{1/2}\right] \tag{3}$$

A quick calculation can be made for the case of Cu^{2+} deposition from aqueous solution based on published molar absorptivities [51, 52]. If one takes a typical photodiode array (PDA) with 2.5 mm × 25 μm pixels which hold approximately 8.5×10^7 photons, employs a 300 μm He–Ne laser, and expands the beam by 8.3 × to utilize the full width of the PDA pixels, the minimum detectable aqueous [Cu^{2+}] is approximately 236 ppb for one scan.

Optical probes based on either refractive index gradients or direct absorption measurements can be employed in principle to monitor the evolution of the mass transfer boundary layer and thus measure the diffusivity of depositing species. This is accomplished by holding the electrode potential anodic of deposition and applying a cathodic potential step to initiate deposition. Diffusivities have been reported in several studies of the boundary layer evolution by both interferometry [53–55] and probe beam deflection [56]. A simple approximation is that the boundary layer thickness δ evolves as

$$\delta = \sqrt{\pi D t} \tag{4}$$

where D is the diffusivity and t the time. However, this expression does not apply when the of convection limits the boundary layer thickness. In this case a more exact solution of Fick's second law yields an infinite series [54, 57, 58]:

$$\Delta C(x,t) = \frac{iv\delta}{nFD}\left\{\left(1 - \frac{x}{\delta}\right) - \frac{8}{\pi^2}\sum_{m=1}^{\infty}\frac{1}{2m-1} \exp\left[-\frac{(2m-1)^2\pi^2 D}{4\delta^2}t\right]\cos\left[\frac{(2m-1)\pi x}{2\delta}\right]\right\} \tag{5}$$

Where m is summation index, i is current density and v is stoichiometric coefficient. Interferometry has also been employed to qualitatively study the evolution of the boundary layer as a function of cell depth, electrode orientation, electrolyte concentration and temperature [59]. Boundary layer growth during electroless deposition is more difficult to study due to solution–phase reactions which can cause bulk concentration gradients, making choice of a reference frame difficult during interferometric investigations [60]. However, one such study of electroless deposition of $CuInSe_2$ has been performed [60], reporting that development of the boundary layer is completed in approximately 300 seconds, longer than is typically observed during electrodeposition [54]. In principle, all of the optical techniques described in this section could similarly be employed to monitor the boundary layer evolution but have instead been applied primarily to coupled reaction-diffusion redox systems. Although photothermal deflection spectroscopy (PDS) has not been employed to study mass transfer in electrochemical systems, its submonolayer sensitivity as a sensor to detect underpotential deposition (UPD) has been demonstrated [61–63].

More detailed studies of mass transfer during electro- and electroless deposition can also be performed. Mass transfer in the microscopic pores of porous electrodes is difficult to study due to the rapidity with which equilibrium is established. An ingenious study by Cairns and co-workers employed probe beam deflection in a model Zn pore to study concentration gradients of zincate ion during dissolution. Numerical solution of the transport equations produced a quantitative fit allowing prediction of the local current density within a model rectangular 500 μm × 200 μm pore [64, 65]. In principle, this approach can similarly be employed for deposition processes. Natural convection has been investigated by several groups using both interferometry [66–72] and spatially resolved absorption spectroscopy [73]. O'Brien and co-workers reported an interferometric study of Zn deposition from $ZnSO_4$ onto a C electrode chosen in order to minimize the effects of the substrate's original morphology. They

reported that for some electrode geometries, the growth rate of the mass transfer boundary layer appeared to vary with deposit morphology(homogeneous, dendritic or fractal) as a result of natural convective effects [72].

Kondo and coworkers have performed the most detailed study of natural convection by optical methods, examining the effect of migration on natural convection by measurement of the concentration profiles of Cu^{2+} in $CuSO_4$ and $CuSO_4/H_2SO_4$ aqueous solutions near a vertical cathode [73]. Concentration profiles as a function of current density for Cu^{2+} are shown in Fig. 1 at a bulk concentration of 0.05 M. These investigators quantified the dependence of Cu^{2+} profile on H^+ migration towards the cathode and the subsequent damping of natural convection with a quantity, f,

$$f = \left(\frac{Ra}{Ra'}\right) \tag{6}$$

where Ra is the Rayleigh number. The primed quantity refers to $CuSO_4$ electrolytes and the unprimed quantity to mixed $CuSO_4/H_2SO_4$ electrolytes. Since the Rayleigh number expresses the ratio of the convective mass transfer rate due to natural convection to the diffusive mass transfer rate, f represents the contribution of migration to the convective mass transfer rate due to the change in buoyancy introduced by the presence of the background electrolyte (H_2SO_4). Concentration profile measurements were fit to numerical solution of the transport equations to determine an f value of approximately 1.19 [73].

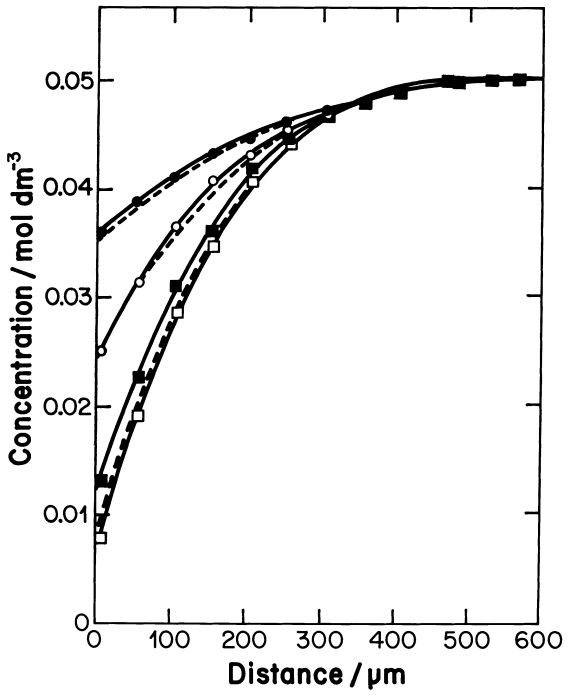

Fig. 1. Cu^{2+} concentration profiles in the boundary layer at a $CuSO_4$ concentration of 0.05 M for current densities $i =$ 0.946 mA cm^{-2} (●), $i = 1.84$ mA cm^{-2}(○), $i = 3.65$ mA cm^{-2} (■), and $i = 4.60$ mA cm^{-2}(□). Reproduced with kind permission from [73].

3. Optical probes of deposit morphology

3.1. *X-ray spectroscopic and diffraction techniques*

X-ray studies of metal deposition can be performed by spectroscopic and diffractive methods to obtain information about the bond lengths and the two-dimensional geometric structure and charge state of the deposit. X-ray absorption near-edge spectroscopy (XANES) employs radiation near the valence edge to promote a core electron to an unoccupied excited state or to a low-lying continuum state. This can be used to probe the valence state of underpotentially deposited species by comparison of the XANES underpotential spectrum and those of related model compounds. An example is provided by studies of UPD Cu on Au(1 0 0), where the XANES spectrum of a UPD monolayer was compared to the XANES spectra of aqueous $CuCl_2$, Cu_2O and Cu foil [74]. This comparison demonstrated that the adsorbed Cu species was close to the +1 oxidation state, revealing considerable charge transfer to the Au substrate [74].

The most commonly employed spectroscopic method is extended X-ray absorption fine structure (EXAFS), which employs X-ray absorption spectroscopy tens to hundreds of electron volts above the absorption edge, where the absorption coefficient oscillates due to interactions with the fields of neighbouring atoms. EXAFS can be made interface sensitive by employing incidence angles of approximately 0.5°, thus reducing the X-ray penetration depth to about 2 nm [75]. The glancing angle geometry also serves to increase the electric field at the surface. Additional surface sensitivity can be achieved by use of a photocathode ionization detector, since the high ionization potential of He suppresses the signal arising from bulk processes, which suffer greater attenuation [7]. EXAFS can be employed either as a probe of electronic energy levels, or, by Fourier transformation of the signal to Cartesian space, as a probe of the local radial structure function. From the latter analysis, the interatomic spacings of near neighbours can be extracted.

Although local order can be probed effectively by EXAFS, such experiments are difficult to perform due to the need for synchrotron or other costly X-ray sources. Information about long-range order can be extracted much more easily from conventional transmission (Laue) and reflection (Bragg) X-ray diffraction experiments [76]. As with EXAFS, the experiments are not inherently surface sensitive but can be made so by employing a glancing angle geometry. For maximum sensitivity at the metal–electrolyte interface, one should operate at an incidence angle greater than the critical angle for the air–electrolyte interface (0.2° at 0.1534 nm) but near the critical angle for the metal–electrolyte interface (0.6°) [77].

X-ray diffraction has provided extensive structural information about interfacial ordering during the initial stages of electrodeposition of a foreign metal.

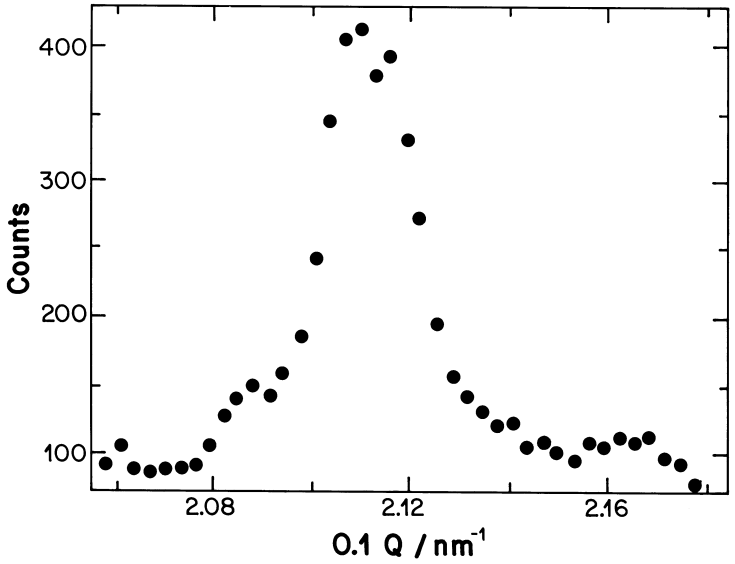

Fig. 2. Radial X-ray diffraction scan of the (1 0) reflection from Pb/Ag(1 1 1) with $\phi = 4.5°$ and $\alpha = \delta = 0.8°$ at −425 mV. Reproduced with kind permission from [78].

Studies of Pb on Ag(1 1 1) by Melroy's group have shown that Pb deposits in an underpotential monolayer which is compressed by approximately 1.4% relative to bulk Pb when deposited at a potential near the underpotential peak [77, 78]. Figure 2 shows a typically narrow diffraction peak obtained in this study. This compression increases to 2.8% as the potential is moved to that appropriate for bulk Pb deposition. Figure 3 illustrates the variation of this compression with electrode potential. These studies have also revealed aspects of morphological development during the initial stages of bulk deposition. Due to the large lattice strain in the epitaxial underpotential layer, multilayer growth occurred as islands, demonstrating the Stranski–Krastonov growth mode for Pb electrodeposition onto Ag(1 1 1). After deposition of what would be five monolayers were the deposit epitaxial, the first monolayer was seen to reconstruct to relieve stress arising from lattice mismatch. The width of the first-order diffraction peak ($0.0037\,\mathrm{nm}^{-1}$) indicates that the size of the ordered domains must be larger than 15 nm [77]. The linewidth can be related to the average domain size D by the approximation [79]:

$$FWHM = \frac{0.9\,\lambda}{D\cos\theta} \tag{7}$$

where θ is the incidence angle and *FWHM* is the true full-width at half-maximum. The observed linewidth is a convolution of the true linewidth and the instrument response function. In addition, more complex methods for relating the linewidth to the domain size have been developed [80].

To address the origins of interfacial ordering, detailed comparative X-ray diffraction studies were performed of Pb and Tl on Au(1 1 1) and Ag(1 1 1) in

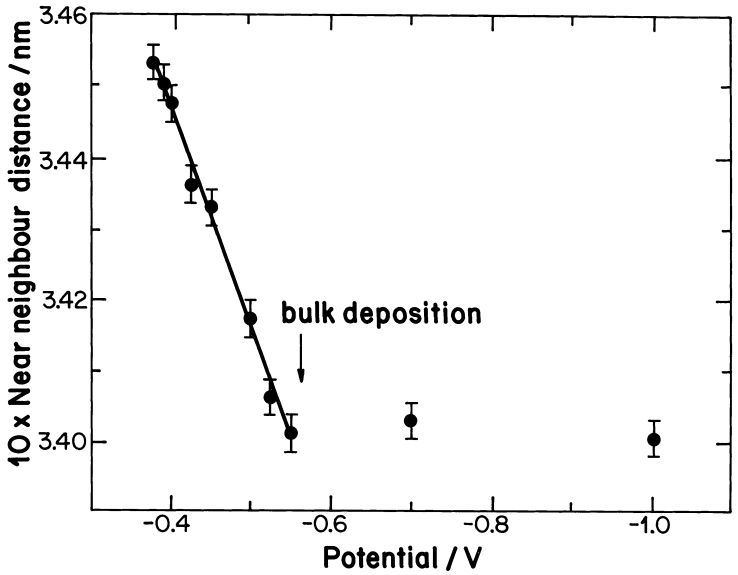

Fig. 3. The variation of Pb–Pb nearest-neighbour distance with potential on Ag(1 1 1). Reproduced with kind permission from [78].

acetate and perchlorate electrolytes. These revealed compressed, incommensurate monolayers whose structure is determined by adatom–adatom interactions rather than adatom-substrate interactions or anion coadsorption effects [81]. Thus interfacial ordering of underpotential Pb may be largely independent of the substrate and the electrolyte.

Copper on Au(1 1 1) is another interesting and complex underpotential system to whose understanding both X-ray diffraction and EXAFS have made significant contributions [82–87]. EXAFS studies of a full monolayer of Cu/Au(1 1 1) indicated that the adlayer was commensurate with the substrate in a 1×1 arrangement [82]. Early studies suggested that the structure of the underpotential layer was dependent on the coverage, on time, and on the direction of the potential scan [83], passing through a stable $(\sqrt{3} \times \sqrt{3})$ R30° structure prior to development of a full monolayer. This $(\sqrt{3} \times \sqrt{3})$R30° structure has been observed by a number of groups and thoroughly studied by a wide variety of methods, including cyclic voltammetry, chronocoulometry, scanning tunnelling microscopy, atomic force microscopy, Fourier transform infrared spectroscopy, quartz crystal microbalance, X-ray diffraction, and EXAFS and XANES [88]. These studies yield evidence for coadsorption of sulfate species but initially yielded no consensus on the structure and composition of the adlayer. This puzzle was finally solved largely due to X-ray diffraction [86] and XANES [87] data demonstrating that the $(\sqrt{3} \times \sqrt{3})$ R30° pattern actually arises from an oxygen atom protruding from an adsorbed sulfate anion, with the Cu atoms forming a honeycomb structure adsorbed onto threefold hollow sites and the sulfate anions occupying the honeycomb centres. The radial structure function for $(\sqrt{3} \times \sqrt{3})$ R30° Cu/Au(1 1 1) obtained from inversion of an EXAFS spectrum is shown in Fig. 4.

3.2. *Ellipsometry*

The rather complex principles of ellipsometry have been reviewed and will be discussed only briefly here [8, 9]. In ellipsometry, polarized and typically monochromatic light is reflected from a surface and the change in polarization state measured. Elliptically polarized light is usually employed, lending the technique its name. Ellipsometry is sensitive to the presence of extremely thin films and to surface morphology, and it is unaffected by the presence of an electrolyte, allowing experimentally straightforward investigation of the thickness and morphology of electrodeposited thin films.

Ellipsometry generally yields a pair of physical parameters Ψ and Δ, which can be related to the amplitude and phase of the incident and reflected radiation as [8, 9]

$$\tan \Psi = \frac{|E_p|}{|E_s|} \quad 0^\circ \leq \Psi \leq 90^\circ \tag{8}$$

$$\Delta = \varepsilon_p - \varepsilon_s \quad 0^\circ \preceq \Delta \preceq 360^\circ \tag{9}$$

These parameters are derived from measured values of the polarization ratio ρ, which is the ratio of the reflection coefficients for the parallel (r_p) and perpendicular (r_s) polarizations according to the following definitions:

$$r_p = \frac{E_p^r}{E_p^i} = \frac{|E_p^r|}{|E_p^i|} e^{i(\varepsilon_p^r - \varepsilon_p^i)} \tag{10}$$

$$r_s = \frac{E_s^r}{E_s^i} = \frac{|E_s^r|}{|E_s^i|} e^{i(\varepsilon_s^r - \varepsilon_s^i)} \tag{11}$$

$$\rho = \frac{r_p}{r_s} = \frac{|E_p^r||E_s^i| e^{i(\varepsilon_p^r - \varepsilon_s^r)}}{|E_p^i||E_s^r| e^{i(\varepsilon_p^i - \varepsilon_s^i)}} \tag{12}$$

where the s and p electric field components of a travelling light wave are represented by an amplitude and a phase as

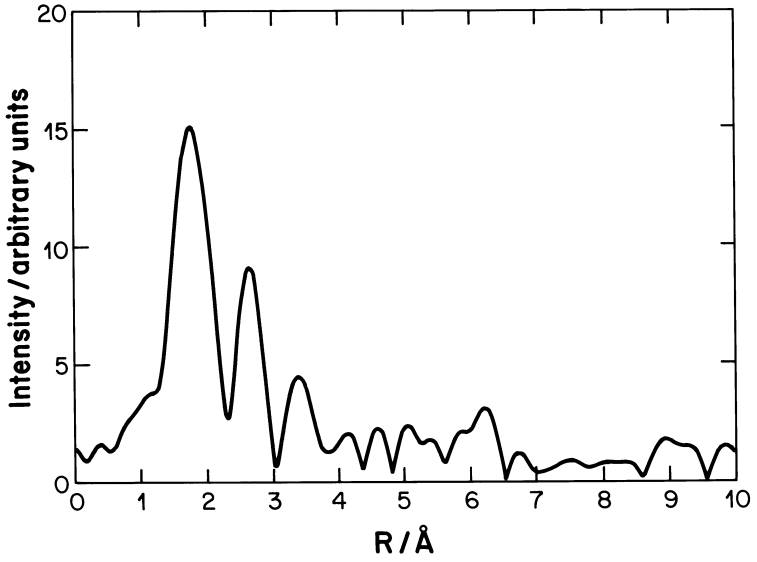

Fig. 4. A Submonolayer radial structure function inverted from the EXAFS spectrum for Cu/Au(1 1 1). Reproduced with kind permission from [85].

$$E_p = |E_p| e^{i\varepsilon_p} \quad (13)$$

$$E_s = |E_s| e^{i\varepsilon_s} \quad (14)$$

By combining Equations 8, 9 and 12 one obtains the basic equation of ellipsometry,

$$\rho = (\tan \Psi) e^{i\Delta} \quad (15)$$

During *in situ* ellipsometric investigation of an electrodeposited thin film, two interfaces must be considered, that between the substrate and film and that between the film and electrolyte. The optical signal detected arises from multiple internal reflections, and the overall reflection coefficients (r_s, r_p) depend on the reflections coefficient of each interface separately $(r_{1s}, r_{1p}, r_{2s}, r_{2p})$ as well as the phase delay D during the propagation through the film [8, 9]

$$r_p = \frac{E_p^r}{E_p^i} = \frac{r_{1p} + r_{2p} e^{-iD}}{1 + r_{1p} r_{2p} e^{-iD}} \quad (16)$$

$$r_s = \frac{E_s^r}{E_s^i} = \frac{r_{1s} + r_{2s} e^{-iD}}{1 + r_{1s} r_{2s} e^{-iD}} \quad (17)$$

where

$$D = \frac{4\pi}{\lambda_0} L n_f \cos \phi_f \quad (18)$$

Here L is the film thickness, n_f the film refractive index, ϕ_f the film angle of refraction, and λ_0 the wavelength of light. By substituting Equations 16 and 17 into Equation 15, one obtains the basic ellipsometry equation for thin film growth,

$$\rho = \frac{(r_{1p} + r_{2p} e^{-iD})(1 + r_{1s} r_{2s} e^{-iD})}{(r_{1s} + r_{2s} e^{-iD})(1 + r_{1p} r_{2p} e^{-iD})} = (\tan \Psi) e^{i\Delta} \quad (19)$$

If the optical constants of the film, substrate and electrolyte and the film thickness, are known Equation 19 allows calculation of the ellipsometry parameters Ψ and Δ. The application of electromagnetic theory to the reflection of light and to the relationship between ellipsometry parameters and thin film optical properties and morphology has been discussed in detail previously [89–92]. With some assumptions and significant analysis, such parameters as the film thickness, film index of refraction, extent of islanding and surface roughness can be individually extracted from ellipsometry data. This will be explored further by discussion of a few published ellipsometry studies.

Yeager and coworkers have employed ellipsometry in an elegant determination of the charge state of Pb underpotentially deposited on Au thin film electrodes [93]. An open question existed at the time regarding the nature of Pb underpotential deposition. Two underpotential peaks were observed, and a controversial explanation of the more cathodic peak suggested that it arose from a charge transfer transition unaccompanied by further Pb deposition. Experimental observables in the form of the polarizer offset from null and the analyser setting, which can be related to the ellipsometry parameters Δ and Ψ, were recorded [94]. These two parameters plus the reflectivity were recorded as a function of electrode potential and excitation wavelength both anodic and cathodic of the voltammetry peak in question.

The complex refractive index and the film thickness were then fitted to the experimental observables with a three-layer model of the system using a nonlinear regression to minimize the difference between the experimental and theoretical values of the ellipsometry observables. The model assumes that the film forms sharp interfaces with both the substrate and electrolyte, both of which are modelled by their bulk properties [93]. This clearly assumes that the optical properties of the substrate surface layer and the electrical double layer and diffuse layer do not differ from those of the bulk phase [95]. This assumption plus the effects of surface roughness provide theoretical limitations to their analysis. The application of a model involving more than three phases is formidable due to the number of optical constants involved. In theory, this problem can be circumvented by measurements at multiple angles of incidence. However, the new equations added to the solution are expected to be nearly linearly dependent. Thus a more exact solution would require determination of the experimental observables more precisely than is currently feasible [95].

The most important result obtained by Yeager and coworkers was that the effective thickness of the underpotential layer was approximately 0.15 nm both at potentials just cathodic and those just anodic of the voltammetry peak in question. This confirms the hypothesis that this peak arises from charge transfer without further deposition. This can be interpreted as evidence for initial incomplete charge transfer during the more anodic peak resulting in an ionic adlayer, followed by full charge transfer during the more cathodic peak. This hypothesis is supported by the strong wavelength dependence of the film's complex index of refraction as well as the large value of the complex component of the index of refraction.

Another example of the use of ellipsometry to study electrodeposition is provided by Farmer and Muller's investigations of Pb deposition on Cu with and without the addition of the model inhibitor Rhodamine-B [96]. This study found that the ellipsometry parameters obtained for a multilayer Pb deposit did not match theoretical predictions of a single film model for either a uniform deposit, a porous deposit, or a deposit consisting of islands with bare substrate patches. Therefore, a model consisting of a uniform underpotential Pb layer underneath a porous bulk deposit was postulated. The porous deposit was treated as one optical component consisting of a mixture of Pb and H_2O with properties calculated from the Bruggeman theory for a binary mixture [96]. Minimization of the difference between the experimental ellipsometry parameters and those obtained from this model yielded a vastly improved data fit (see Fig. 5) and provided estimates for the thickness and porosity of the bulk deposit. Without the presence of the model inhibitor, the bulk deposit

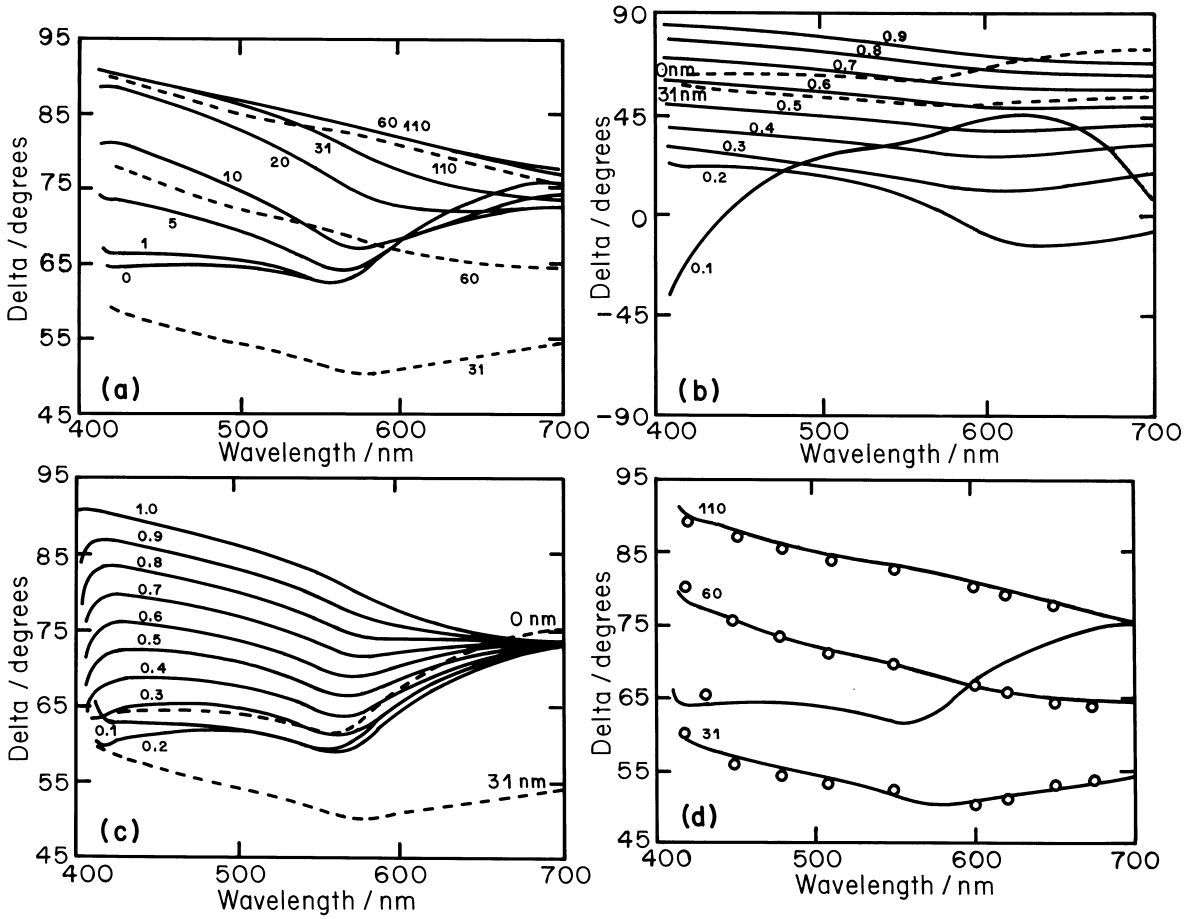

Fig. 5. Experimental fit of the ellipsometry parameter delta to model calculations for an (a) uniform deposit, (b) porous deposit, (c) island deposit, and (d) porous deposit atop a uniform underpotential deposit. Curves are labelled with the deposit thickness (nm) or the fractional submonolayer coverage. Reproduced with kind permission from [96].

showed porosities of 41%, 22% and 3% for film thicknesses of 30, 60 and 110 nm [96]. The addition of the inhibitor decreased the porosity of a 30 nm film to about 10%, almost completely masking the Cu substrate.

No universally accepted theoretical interpretation exists for ellipsometry data. Bulk optical constants are often assumed for monolayer thick films, clearly a questionable assumption. In addition, real interfaces are never sharp, as evidenced by the electrical double layer and diffuse layer in solution and the effects of crystalline anisotropy on the metal side. The effects of interfacial roughness are also difficult to include in a physically meaningful way. In practice different models can be tested until agreement with experiment is obtained, so ellipsometry should be regarded as a useful but not rigorous method. For electrodeposited films much thicker than a monolayer, ellipsometry should provide consistent and reliable thickness measurements.

4. Optical probes of surface vibrational structure

To the author's knowledge, no vibrational spectra of metal species at an electrode surface have been recorded. Thus metal deposition can be studied only indirectly by vibrational spectroscopy.

4.1. *Surface-enhanced Raman spectroscopy*

Raman spectroscopy is a probe of vibrational structure where light of frequency ω_{inc} is scattered by the sample and light of frequency $\omega_{inc} \pm \omega_{vib}$ is detected, where ω_{vib} matches a vibrational frequency of the system. Surface enhancement occurs when noble metal surfaces are electrochemically roughened by oxidation–reduction cycles, producing active sites which are believed to be small clusters of atoms. These active sites increase the transition intensity by a combination of two effects, the electromagnetic enhancement mechanism, whereby the roughened surface increases the strength of the local electric field, and a chemical mechanism associated with quantum electronic effects involving the adsorbate and surface electronic energy states [1–3]. Although practical surface-enhanced Raman spectroscopy (SERS) is limited mainly to Ag, Au and Cu electrodes, in theory any small molecule which will adsorb on those surfaces can be studied. The generality of SERS can be expanded somewhat by obtaining SERS spectra on gold electrodes onto which other metals have been underpotentially deposited [97].

A practical difficulty of SERS studies is the separation of the Raman frequency of interest from the enormous Rayleigh background at the incident

frequency. Since this background signal is many orders of magnitude more intense than the Raman signal, the high vibrational frequencies observed in small adsorbed species are easier to separate from the background signal, since $\omega_{vib} \propto m^{-1/2}$. Primarily for this reason the Raman spectra of metal species have not to the author's knowledge been recorded. Other difficulties include the transition intensity and the uncertain microstructural effects of the roughening process.

A straightforward method for studying metal deposition is to omit the roughening process and instead study the surface after natural roughening occurs during electrodeposition [98–100]. The morphological development can be followed indirectly by monitoring a vibrational transition of an adsorbed species such as the CN^- stretch which should be sensitive to the local chemical environment. The evolution of the CN^- stretch intensity at approximately 2110 cm^{-1} during deposition of Ag onto Pt as observed by Plieth is shown in Fig. 6. The temporal spectral evolution could be related qualitatively to nucleation phenomena during Ag growth. In another study the CN^- stretch was seen to be split into several peaks after a double pulse roughening procedure [98]. This arises from heterogeneity in the local environment, suggesting that different cluster sizes are responsible for different peaks. These investigators argued that a vibrational normal mode analysis could not explain the data and proposed that the effect arises from variation of the cluster charge density with size. Although such studies do not yet allow quantitative analysis, they demonstrate the potential usefulness of SERS for monitoring morphology evolution during electrodeposition. Since plating baths often contain small molecular species such as CN^- real plating systems might be studied *in situ*.

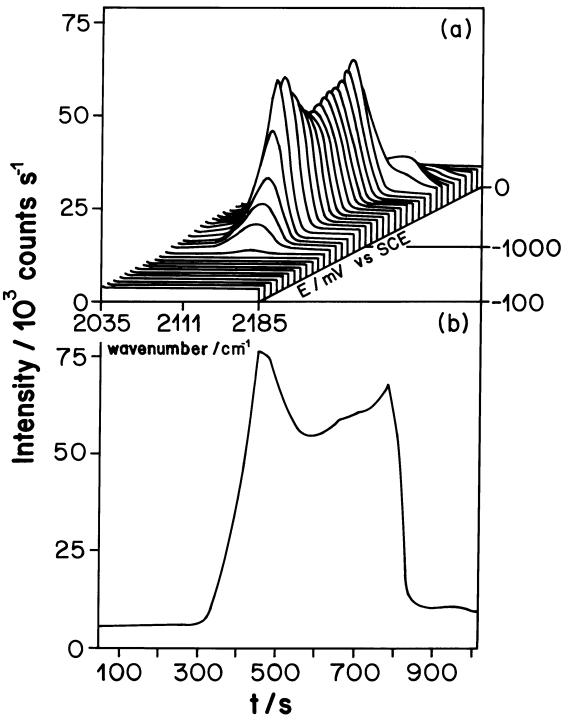

Fig. 6. Development of the CN^- stretch vibration during Ag growth on Pt with a potential cycle 0 V → −1.0 V → 0 V, showing (a) a three-dimensional representation and (b) a slice at 2111 cm^{-1}. Reproduced with kind permission from [99].

SERS can also be employed to investigate metal deposition through studies of the effects of plating bath additives, such as nicotinic acid, thiourea and polyethylene glycol [101–103]. Although plating bath additives are widely employed as levelling and brightening agents, their modes of action are complex and not fully understood [104, 105]. Since many theoretical interpretations of the action of additives involve adsorption onto the electrode surface, SERS can be an ideal method to study the mechanistic behaviour of additives. SERS studies have yielded evidence that as the electrolyte is made more basic, nicotinic acid changes its surface orientation from primarily parallel to nearly perpendicular to a Ag surface [103]. The opposite change in orientation has been suggested for thiourea as the electrode potential becomes increasingly negative [102]. Evidence for this shift in orientation can be seen graphically in Fig. 7, where the SCCN out-of-plane bending vibration at 610 cm^{-1} becomes more intense at negative potentials. This change has been related to catalytic effects of thiourea on hydrogen evolution [102]. SERS alone is incapable of addressing the difficult question of the mode of action of plating additives, but may play an important role in conjunction with other analytical techniques.

4.2. *Infrared absorption spectroscopy (IRAS)*

When the photon energy matches a vibrational frequency on the surface and when symmetry requirements are satisfied, an infrared absorption peak may be observed. An additional condition which must be met is that a change in this vibrational quantum state must be accompanied by a significant change in the dipole moment in the same direction as the exciting electric field vector. IRAS has only recently become widely applicable to electrochemical interfaces due to numerous experimental difficulties, including the strong absorption of infrared light by H_2O, necessitating the use of thin layer cells. However, the main difficulty is the extremely low intensity of most surface infrared transitions due to both the intrinsically small transition dipole moment and the low density of sites on the surface relative to the bulk electrolyte. Early attempts to increase the sensitivity by electrode potential modulation have been greatly facilitated by the use of modern Fourier transform spectrometers [4–6].

IRAS studies of small molecules adsorbed onto underpotential deposition systems can yield information about charge distribution on the surface, as can be illustrated by studies of sulfate and bisulfate adsorption on underpotentially deposited metals. The spectra of sulfate and bisulfate on bare Au and Cu/Au have been obtained as a function of electrode potential and pH in both $CuSO_4$- and H_2SO_4-containing electrolytes

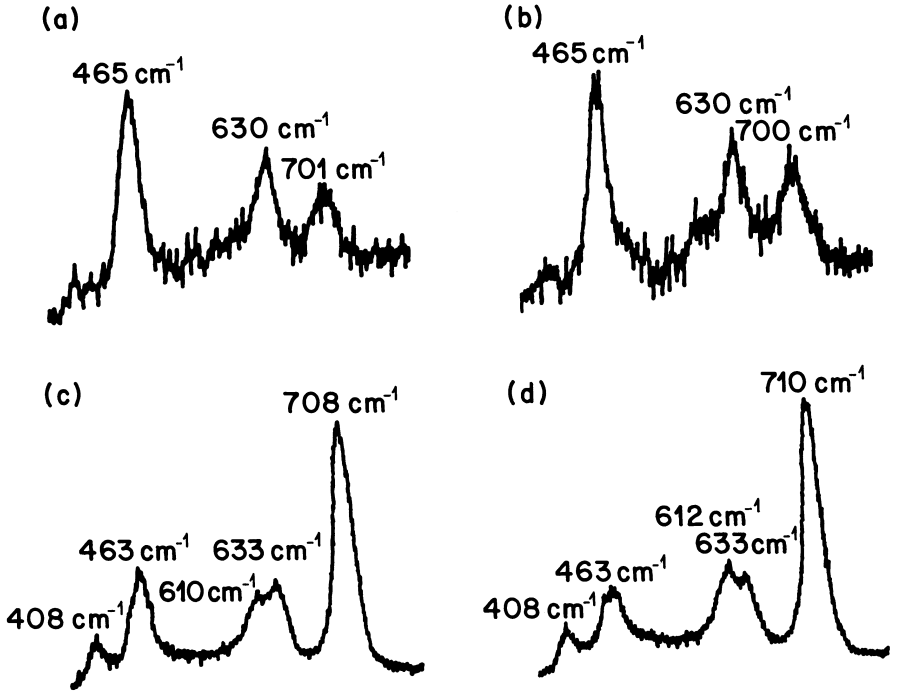

Fig. 7. Raman spectra from a roughened silver electrode in a bath containing 0.01 M $AgNO_3$, 0.01 M thiourea and 0.5 M $HClO_4$ at (a) open circuit, (b) 0.20 V vs SCE, (c) −0.60 V and (d) −0.80 V. Reproduced with kind permission from [100].

[106]. In H_2SO_4 electrolytes at potentials where UPD Cu is deposited, the amount of adsorbed sulfate increases. This has been attributed to a partial positive charge on the UPD adlayer, which favours adsorption of the more negatively charged adsorbate [106]. When the applied voltage becomes sufficiently negative to induce full discharge of the UPD Cu layer, the negative applied potential causes an increase in $[H^+]$ near the interface. This results in a decrease in adsorbed sulfate and an increase in adsorbed bisulfate.

Similar studies have helped elucidate the interfacial structure during Cu underpotential deposition onto Pt(1 1 1). Cu underpotential deposition proceeds through two voltammetric peaks, and it is generally accepted that UPD is initiated during the first peak and completed after the second peak. However, the Cu deposit always shows a $(\sqrt{3} \times \sqrt{3})$ R30° structure in *ex situ* LEED experiments. IRAS studies showed that at a potential above the first voltammetry peak the predominant adsorption peak occurred near 1300–1317 cm^{-1} and between the two voltammetry peaks the predominant IRAS peak occurred near 1252 cm^{-1} [107]. The former IRAS peak was assigned to bisulfate adsorbed directly onto Pt(1 1 1) and the latter peak to bisulfate adsorbed onto the UPD Cu. This and other evidence were best explained by the hypothesis that the sites of the $(\sqrt{3} \times \sqrt{3})$ R30° reconstruction unoccupied by Cu are occupied instead by adsorbed sulfate and bisulfate [107].

5. Optical probes of surface electronic structure

With the advent of major strides in the understanding of surface physics, optical probes of the surface electronic structure such as second harmonic generation (SHG) and electroreflectance could provide useful information about surface morphology and magnetic and other surface properties. At present these methods may be used empirically to monitor film thickness or to monitor the optical properties of deposited films.

5.1. *Second harmonic generation*

Surface second harmonic generation (SHG) is a nonlinear optical process whereby a laser at frequency ω impinges on a surface and light at frequency 2ω is produced and detected. Bulk SHG is forbidden in centrosymmetric media such as metals and electrolyte solutions. Thus in electrochemical systems inversion symmetry is broken and second harmonic generation dipole-allowed only within a thin layer ($\sim$ 1 nm) at the metal–electrolyte and air–electrolyte interfaces. Since the latter signal can usually be neglected, SHG can be a sensitive probe of surface chemistry. For many adsorbed atoms, ions and small molecules, surface SHG has been shown to be highly sensitive to adsorption due to adsorbate-induced variations in the substrate nonlinearity. SHG is often sensitive both to specific adsorption and to species deposited by faradaic processes.

The utility of SHG is limited somewhat by its molecular nonspecificity, making application of SHG to multicomponent systems difficult. This limitation can be circumvented by wavelength-dependent studies which exploit the presence of surface electronic resonances [108]. SHG has seen significant application to studies of adsorption and underpotential deposition processes [10, 11]. For example, Richmond has demonstrated that SHG is strongly sensitive to

underpotential deposition of Tl but only weakly sensitive to underpotential deposition of Cu and Ag on Au(1 1 1) [109]. Tl/Ag(1 1 1) is another interesting system, where the relationship between SHG and surface coverage is discontinuous at about 0.75 monolayer, suggesting the presence of a phase transition [110].

5.2. *Photo- and electroreflectance*

Photo- and electroreflectance are both concerned with the change in the surface optical reflectivity (R) with photon energy. Since for d.c. experiments this change is subtle, the surface electric field (E) is usually modulated and the nth-derivative spectrum (d^nR/dE^n) obtained [12]. This provides a much sharper variation of the spectrum with photon energy, yielding distinct spectral features when the photon energy resonates with surface electronic energy levels. Modulation arises from variation of the electric field in the case of electroreflectance and from illumination with a laser in the case of photoreflectance. In electroreflectance, first derivative spectra are usually taken, and the observed change in the reflectance is normalized to the reflectance and reported as $\delta R/R$ at constant ΔE.

Kolb has studied electroreflectance spectra of single crystal metal electrodes, with and without underpotential deposition. Spectra on Ag(1 1 1) include a sharp resonance at approximately 3.9 eV, whose dependence on incidence angle demonstrates that it arises from an electronic transition involving bound electrons [111]. Electroreflectance can also be employed to study surface plasmons. For a perfectly smooth surface, the surface plasmon resonance at approximately 3.5 eV is not evident in the electroreflectance spectrum. However, its energetic position can be observed as a function of electrode potential if the surface is electrochemically roughened. The results of this investigation show that anodic of the potential of zero charge (PZC), the surface plasmon energy shifts linearly with potential, as can be predicted on the basis of changes in the surface electron density [112].

Kolb has also studied underpotential deposition by monitoring the differential reflectance spectra (DRS), where the reflectance change

$$\frac{\Delta R}{R} = \frac{R(\mathrm{d}) - R(0)}{R(0)} \qquad (20)$$

is measured. Here $R(0)$ is the reflectance of the bare surface and $R(\mathrm{d})$ that of the adsorbate-covered surface. For a simple three-phase model with sharp boundaries, $\Delta R/R$ can be related to the dielectric constants of the electrolyte, film and substrate, although the same problems arise as in ellipsometry. For Cu underpotentially deposited on Pt, DRS spectra show resonances associated with the deposited layer at approximately 2.1, 2.8 and 4.1 eV [113]. The optical constants of the underpotential layer were found to differ substantially from bulk Cu, and previous work showed that for Ag on Pt the optical constants did not equal those for the bulk material until approximately 4–5 monolayers were deposited [114]. When the reflectance change per unit coverage ($\Delta R/R\theta$) is plotted against coverage, a clear discontinuity is seen at $\theta = 2/3$, indicating a structural transition at this coverage. Discontinuities can also be seen in the curve of reflectance against coulombic charge transferred for the case of Tl underpotential deposition of Ag(1 1 1), as shown in Fig. 8 [115].

6. Concluding remarks

At present, optical studies of metal electro- and electroless deposition are confined mainly to academic laboratories. However, numerous technological developments suggest that this situation may change in the near future. As microelectronics interconnects are continually reduced in size, and as other industries adapt the micro- and nanotechnologies originally developed for use in the microelectronics industry, the need to inexpensively deposit metals with microscopic precision will increase. Electro- and electroless deposition of metals have tremendous promise as low-cost alternatives to the vacuum deposition methods more commonly employed today. Nonintrusive *in situ* optical methods which probe the boundary layer composition, deposit morphology, and possibly even surface electronic structure may have an important role in establishing

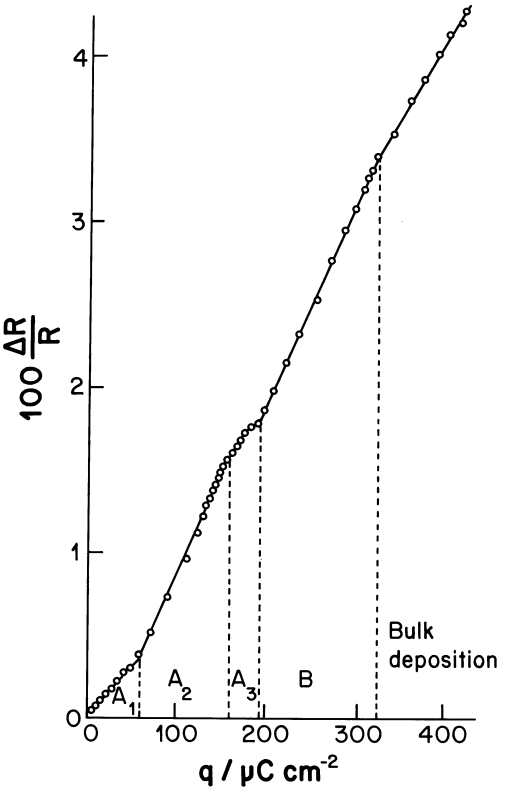

Fig. 8. Variation of the reflectance with coulombic charge passed during UPD of Tl/Ag(1 1 1). Reproduced with kind permission from [115].

the process–structure–function relationships determined in pilot studies of metal deposition with controlled morphology.

References

[1] A. Otto, I. Mrozek, H. Grabhorn and W. Akemann, *J. Phys. Condens. Matter*. **4** (1992) 1143.
[2] R. L. Birke, T. Lu and J. R. Lombardi, *in* 'Techniques for Characterization of Electrodes and Electrochemical Processes' (edited by R. Varma and J. R. Selman), J. Wiley & Sons, New York (1991).
[3] R. K. Chang, *Ber. Bunsenges. Phys. Chem*. **91** (1988) 296.
[4] J. K. Foley and B. S. Pons, *Anal. Chem*. **57** (1985) 954A.
[5] S. Pons, T. Davidson and A. Bewick, *J. Electroanal. Chem*. **160** (1984) 63.
[6] A. Bewick, K. Kunimatsu, B. S. Pons and J. W. Russell, *J. Electroanal. Chem*. **160** (1984) 47.
[7] G. G. Long and J. Kruger, *in* 'Techniques for Characterization of Electrodes and Electrochemical Processes' (edited by R. Varma and J. R. Selman), J. Wiley & Sons, New York (1991).
[8] R. H. Muller, *Adv. Electrochem. Electrochem. Engng* **9** (1973) 167.
[9] R. H. Muller, *in* 'Techniques for Characterization of Electrodes and Electrochemical Processes' (edited by R, Varma and J. R. Selman), J. Wiley & Sons, New York (1991).
[10] R. M. Corn and D. A. Higgins, *Chem. Rev*. **94** (1994) 107.
[11] G. L. Richmond, J. M. Robinson and V. L. Shannon, *Prog. Surf. Sci*. **28** (1988) 1.
[12] D. E. Aspnes, *in* 'Handbook on Semiconductors', Volume 2 (edited by T. S. Moss), North-Holland, New York (1975), p. 109.
[13] D. E. Aspnes, *Surf. Sci*. **37** (1973) 418.
[14] M. Cardona, K. L. Shaklee and F. H. Pollak, *Phys. Rev*. **154** (1967) 696.
[15] J. D. Rudnicki, F. R. McLarnon and E. J. Cairns, *in* 'Techniques for Characterization of Electrodes and Electrochemical Processes' (edited by R. Varma and J. R. Selman), J. Wiley & Sons, New York (1991).
[16] J. D. Rudnicki, G. M. Brisard, H. A. Gasteiger, R. E. Russo, F. R. McLarnon and E. J. Cairns, *J. Electroanal. Chem*. **362** (1993) 55 and references therein.
[17] R. H. Muller, *Adv. Electrochem. Electrochem. Engng* **9** (1973) 281.
[18] E. I. Tochitskii and N. M. Belyavskii, *Phys. Stat. Sol. A* **61** (1980) K21.
[19] I. R. Christie and B. P. Cameron, *Gold Bull*. **27** (1), (1994) 12.
[20] Y. Okinaka, *in* 'Electrodeposition Technology, Theory and Practice' (edited by L. T. Romankiw and D. R. Turner), The Electrochemical Society, Pennington, NJ (1987).
[21] W. J. Dauksher, D. J. Resnick, W. A. Johnson and A. W. Yanof, *Microelectron. Engng* **23** (1994) 235.
[22] G. Franz, *Thin Solid Films* **169** (1989) 105.
[23] W. Mehl and J. O. Bockris, *J. Chem. Phys*. **27** (1957) 818.
[24] *Idem, Can. J. Chem*. **37** (1959) 190.
[25] J. O. Bockris and M. Enyo, *Trans. Far. Soc*. **58** (1962) 1187.
[26] Q. J. M. Slaiman and W. J. Lorenz, *Elec. Acta* **19** (1974) 791.
[27] G. Okada, N. Yamazoe and T. Seiyama, *Denki Kagaku* **44** (1976) 413.
[28] V. V. Trofimenko, I. N. Kosenko, V. P. Zhitnik, V. S. Kovalenko and Y. M. Loshkarev, *Sov. Elec*. **26** (1990) 347.
[29] See *MRS Bull*. **18** (1993) 18–56.
[30] R. Schumacher, J. J. Pesek and O. R. Melroy, *J. Phys. Chem*. **89** (1985) 4338 and references therein.
[31] K. G. Mishra and R. K. Paramguru, *J. Electrochem. Soc*. **143** (1996) 510.
[32] S. Nakahara and Y. Okinaka, *Acta Metall*. **31** (1983) 713.
[33] A. Dziuve and V. Jasulaitiene, *Chemija* **1993** 18.
[34] J. B. deCusminsky and H. Wilman, *Electrochim. Acta* **17** (1972) 237.
[35] K. M. Gorbunova and T. A. Tkachik, *ibid*. **16** (1971) 191.
[36] N. A. Economou, H. Fischer and D. Trivich, *ibid*. **2** (1960) 207.
[37] K. D. Bird and M. Schlesinger, *J. Electrochem. Soc*. **142** (1995) L65.
[38] M. Alper, K. Attenborough, V. Baryshev, R. Hart, D. S. Lashmore and W. Schwarzacher, *J. Appl. Phys*. **75** (1994) 6543.
[39] D. Tench and J. White, *J. Electrochem. Soc*. **137** (1990) 10.
[40] M. Tan, E. Haftek, A. Waknis and J. A. Barnard, *MRS Symp. Proc*. **238** (1992) 695.
[41] J. R. LaGraff and A.A. Gewirth, *J. Phys. Chem*. **98** (1994) 11246 and references therein.
[42] L. E. Fosdick and J. L. Anderson, *Anal. Chem*. **60** (1988) 156.
[43] *Idem*, *ibid*. **60** (1988) 163.
[44] F. R. McLarnon, R. H. Muller and C. W. Tobias, *J. Electrochem. Soc*. **122** (1975) 59.
[45] See *Adv. Electrochem. Electrochem. Engng* **9** (1973).
[46] T. Kuwana and W. R. Heineman, *Accts. Chem. Res*. **9** (1976) 241.
[47] J. F. Tyson and T. S. West, *Talanta* **26** (1979) 117.
[48] *Idem*, *ibid*. **27** (1980) 335.
[49] J. Zak, M. D. Porter and T. Kuwana, *Anal. Chem*. **55** (1983) 2219.
[50] R. B. Bilhorn, P. M. Epperson, J. V. Sweedler and M. B. Denton, *Appl. Spec*. **41** (1987) 1125.
[51] J. Bjerrum, *J. Inorg. Nucl. Chem*. **25** (1963) 315.
[52] J. Bjerrum, C. J. Ballhausen and C. K. Jorgenson, *Acta Scand*. **8** (1954) 1275.
[53] R. N. O'Brien and C. Rosenfield, *J. Phys. Chem*. **67** (1963) 643.
[54] A. Tvarusko and L. S. Watkins, *Electrochim. Acta* **14** (1969) 1109.
[55] F. R. McLarnon, R. H. Muller and C. W. Tobias, *ibid*. **21** (1976) 101.
[56] C. Barbero, M. C. Miras and R. Kotz, *ibid*. **37** (1992) 429.
[57] J. Crank, 'The Mathematics of Diffusion', Oxford University Press, London (1957).
[58] K. J. Vetter, 'Electrochemical Kinetics', Academic Press, New York (1967).
[59] R. N. O'Brien, C. A. Rosenfield, K. Konoshita, W.F. Yakymyshyn and J. Leja, *Can. J. Chem*. **43** (1965) 3304.
[60] R. N. O'Brien, *J. Electroanal. Chem*. **260** (1989) 231.
[61] A. Fujishima, H. Masuda, K. Honda and A. J. Bard, *Anal. Chem*. **52** (1980) 682.
[62] J. P. Roger, D. Fournier and A. C. Boccara, *J. Phys. Coll*. **6** (1983) C-313.
[63] S. Yoshihara, M. Okamoto, K. Endo and E. Sato. 'Interfinish 92', International Congress of Surface Finishing (1992) p. 3 and p. 1434.
[64] J. K. Weaver, F. R. McLarnon and E. J. Cairns, *J. Electrochem. Soc*. **138** (1991) 2572.
[65] *Idem*, *ibid*. **138** (1991) 2579.
[66] N. Ibl, Y. Barrada and G. Truempler, *Helv. Chim. Acta* **37** (1954) 583.
[67] N. Ibl and R. Muller, *Z. Elektrochem*. **59** (1955) 67.
[68] R. N. O'Brien, W. F. Takymshyn and J. Leja, *J. Electrochem. Soc*. **110** (1963) 820.
[69] R. N. O'Brien, *Nature* **201** (1964) 74.
[70] Y. Awakura and Y. Kondo, *J. Electrochem. Soc*. **123** (1976) 1184.
[71] Y. Fukunaka, T. Minegishi, N. Nishioka and Y. Kondo, *ibid*. **128** (1981) 1274.
[72] R. N. O'Brein and K. S. V. Santhanam, *J. Electroanal. Chem*. **352** (1993) 167.
[73] Y. Fukunaka, K. Denpo, M. Iwata, K. Muruoka and Y. Kondo, *J. Electrochem. Soc*. **130** (1983) 2492
[74] A. Tadjeddine, A. Lahrichi and G. Tourillon, *J. Electroanal. Chem*. **360** (1993) 261.
[75] T. E. Furtak, L. Wang, J. Pant, K. Pansewicz and T. M. Hayes, *J. Electrochem. Soc*. **141** (1994) 2369.
[76] M. Fleischmann, A. Oliver and J. Robinson, *Electrochim. Acta* **31** (1986) 899.
[77] M. G. Samant, M. F. Toney, G. L. Borges, L. Blum and O. R. Melroy, *Surf. Sci*. **193** (1988) L29.
[78] O. R. Melroy, M. F. Toney, G. L. Borges, M. G. Samant, J. B. Kortright, P. N. Ross and L. Blum, *J. Electroanal. Chem*. **258** (1989) 403.
[79] B. E. Warren, 'X-ray Diffraction', Dover Publications , New York (1969).
[80] D. Balzar and S. Popovic, *J. Appl. Cryst*. **29** (1996) 16 and references therein.
[81] M. F. Toney, J. G. Gordon, M. G. Samant, G. L. Borges, D. Yee and L. B. Sorensen, *J. Phys. Chem*. **99** (1995) 4733.

[82] O. R. Melroy, M. G. Samant, G. L. Borges, J. G. Gordon, J. H. White, M. J. Albarelli, M. McMillan and H. D. Abruna, *Langmuir* **4** (1988) 728.
[83] A. Tadjeddine, D. Guay, M. Laddouceur and G. Tourillon, *Phys. Rev. Lett.* **66** (1991) 2235.
[84] A. Tadjeddine, G. Tourillon and D. Guay, *Electrochim. Acta* **36** (1991) 1859.
[85] J. G. Gordon, O. R. Melroy and M. F. Toney, *ibid.* **40** (1995) 3.
[86] M. F. Toney, J. N. Howard, J. Richer, G. L. Borges, J. G. Gordon, O. R. Melroy, D. Yee and L. B. Sorensen, *Phys. Rev. Lett.* **75** (1995) 4472.
[87] S. Wu, J. Lipkowski, T. Tyliszczak and A. P. Hitchcock, *Prog. Surf. Sci.* **50** (1995) 227.
[88] J. Zhang, Y. E. Sung, P. A. Rikvold and A. Wieckowski, *J. Chem. Phys.* **104** (1996) 5699 and references therein.
[89] R. M. A. Azzam and N. M. Bashara, 'Ellipsometry and Polarized Light', North-Holland, Amsterdam (1977).
[90] M. Born and E. Wolf, 'Principles of Optics', 2nd edn, MacMillan, New York (1964).
[91] J. Van Kranendank and J. E. Sipe, *Prog. Opt.* **15** (1977) 247.
[92] P. H. Berning, *Phys. Thin Films* **1** (1963) 69.
[93] J. Horkans, B. D. Cahan and E. Yeager, *J. Electrochem. Soc.* **122** (1975) 1586.
[94] B. D. Cahan, J. Horkans and E. Yeager, *Surf. Sci.* **37** (1973) 559.
[95] J. Horkans, B. D. Cahan and E. Yeager, *ibid.* **46** (1974) 1.
[96] J. C. Farmer and R. H. Muller, *J. Electrochem. Soc.* **132** (1985) 313.
[97] L. W. H. Leung and M. J. Weaver, *J. Electroanal. Chem.* **217** (1987) 367.
[98] B. Reents, G. Lacconi and W. Plieth, *ibid.* **376** (1994) 185.
[99] G. Lacconi, B. Reents and W. Plieth, *ibid.* **325** (1992) 207.
[100] M. Fleischmann, G. Sundholm and Z. Q. Tian, *Electrochim. Acta* **31** (1986) 907.
[101] J. P. Healy, D. Fletcher and M. Goodenough, *J. Electroanal. Chem.* **338** (1992) 155.
[102] Z. Q. Tian, Y. Z. Lian and M. Flieschmann, *Electrochim. Acta* **35** (1990) 879.
[103] W. Plieth, *ibid.* **37** (1992) 2115.
[104] L. Oniciu and L. Muresan, *J. Appl. Electrochem.* **21** (1991) 565.
[105] T. C. Franklin, *Surf. Coat. Technol.* **30** (1987) 415.
[106] D. B. Parry, M. G. Samant, H. Seki, M. R. Philpott and K. Ashley, *Langmuir* **9** (1993) 1878.
[107] H. Ogasawara, J. Inukai and M. Ito, *Surf. Sci.* **311** (1994)L665.
[108] R. A. Bradley, R. Georgiadis, S.D. Kevan and G.L. Richmond, *J. Chem. Phys.* **99** (1993) 5535.
[109] D. A. Koos and G. L. Richmond, *J. Phys. Chem.* **96** (1993) 3770.
[110] D. A. Koos, V. L. Shannon and G. L. Richmond, *J. Phys. Chem.* **94** (1990) 2091.
[111] D. M. Kolb, *J. Phys. Colloq.* **C5** (1977) 167.
[112] D. M. Kolb and R. Kotz, *Surf. Sci.* **64** (1977) 96.
[113] *Idem, ibid.* **64** (1977) 698.
[114] J. D. E. McIntyre and D. M. Kolb, *Symp. Faraday Soc.* **4** (1970) 99.
[115] A. Bewick and B. Thomas, *J. Electroanal. Chem.* **65** (1975) 911.